NJC

LETTER

View Article Online
View Journal | View Issue

Published on 30 July 2015. Downloaded by Nanjing Normal University on 09/01/2018 13:04:51.

Cite this: *New J. Chem.*, 2016, **40**, 914

Received (in Montpellier, France) 27th June 2015, Accepted 30th July 2015

DOI: 10.1039/c5nj01659b

www.rsc.org/njc

Polyoxometalate-assisted fabrication of the Pd nanoparticle/reduced graphene oxide nanocomposite with enhanced methanol-tolerance for the oxygen reduction reaction†

Ji-Sen Li,[ab] Hui-Qing Dong,[b] Shun-Li Li,[b] Run-Han Li,[b] Zhi-Hui Dai,*[b] Jian-Chun Bao[b] and Ya-Qian Lan*[b]

A polyoxometalate (POM)-assisted fabrication of Pd nanoparticle/reduced graphene oxide (rGO) nanocomposite is reported. The hybrid exhibits enhanced catalytic activity and excellent methanol-tolerance capacity compared to its counterparts, due to the synergistic effect of Pd, POM, and rGO.

In recent years, direct methanol fuel cells (DMFCs), a class of proton exchange membrane fuel cells, have received considerable attention for energy storage and conversion due to their unique properties such as high power density, low to zero emission and simple processing.[1] Nevertheless, there are some problems still preventing the commercialization of DMFCs, including the sluggish kinetics, high cost of Pt or Pt-based catalysts for oxygen reduction reaction (ORR) at the cathode, and methanol crossover through the membrane.[2] Hence, it is an urgent need to search for novel catalysts with lower cost, high efficiency, and excellent methanol-tolerance.

In this regard, Pd-based catalysts,[3] as promising alternatives, have been the focus of recent research for ORR, because they have a relatively high electrocatalytic activity, even comparable to that of the Pt–C catalyst, and their cost are lower than that of Pt–C. In addition, to further improve the catalytic performance of Pd nanoparticles (Pd NPs), a suitable support for the dispersity of Pd NPs is expected to exploit. Reduced graphene oxide (rGO), as a new support material, has been actively investigated because of its excellent electron transport property and chemical stability.[4] But they are usually aggregated due to strong π-stacking and hydrophobic interactions, which impede the practical applications.[5] In parallel, polyoxometalates (POMs),[6] consisted of oxygen and transition-metal atoms, have attracted much interest due to their versatile physical and chemical properties, which are applied for catalysis, electrochemistry, energy storage, and so on. However, their applications are immensely limited because of their lower surface area and higher solubility in aqueous solution. Fortunately, due to the chemisorption interaction between carbon materials and POMs,[7] the POM/rGO hybrid may not only overcome the above-mentioned shortcomings of POMs and rGO, but also significantly improve the electrocatalytic activity.[8] Inspired by the merits of Pd NPs and the POM/rGO hybrid, we speculate that a novel metal nanoparticle/POM/rGO composite is promising, which may exhibit further improved electrocatalytic activity and methanol-tolerance capacity. To date, to the best of our knowledge, only a limited number of metal naoparticle/POM/carbon composites as catalysts have been reported.[9] But the synthesis and application of porous Pd/POM/rGO composites by the assistance of POMs have not been explored for ORR so far. Therefore, it is a challenging task to fabricate a novel Pd/POM/rGO hybrid as an excellent electrocatalyst for ORR in DMFCs.

Herein, for the first time, we report a POM-assisted fabrication of a Pd/PMo12/rGO nanocomposite using $Pd(NO_3)_2$, phosphomolybdic acid (PMo12), and graphene oxide as precursors (Scheme 1), which was served as an electrocatalyst for ORR in an acid medium. The influence of the contents of Pd on the ORR was systematically investigated. The catalytic activity of Pd/PMo12/rGO is higher than its counterparts. Most importantly, the composite possesses outstanding methanol-tolerance, which is important for practical applications of DMFCs.

The transmission electron microscopy (TEM) images of the Pd/PMo12/rGO composite at different magnifications are shown in Fig. 1a–c. The Pd NPs are uniformly dispersed or decorated on the wrinkled surfaces of rGO. From statistical analysis (inset of Fig. 1a), the average size of Pd is about 2.38 nm. The high-resolution TEM (HRTEM) image (inset of Fig. 1b) reveals that the fringe spacing of Pd is 0.226 nm. These results

[a] *Key Laboratory of Inorganic Chemistry in Universities of Shandong, Department of Chemistry and Chemical Engineering, Jining University, Qufu, 273155, Shandong, P. R. China*

[b] *Jiangsu Key Laboratory of Biofunctional Materials, College of Chemistry and Materials Science, Nanjing Normal University, Nanjing 210023, P. R. China. E-mail: yqlan@njnu.edu.cn, daizhihuii@njnu.edu.cn*

† Electronic supplementary information (ESI) available: Experimental section, and additional figures and table. See DOI: 10.1039/c5nj01659b

 This journal is © The Royal Society of Chemistry and the Centre National de la Recherche Scientifique 2016

Published on 30 July 2015. Downloaded by Nanjing Normal University on 09/01/2018 13:04:51.

Scheme 1 Preparation procedure of a novel Pd/PMo12/rGO composite. HPB: heteropoly blue.

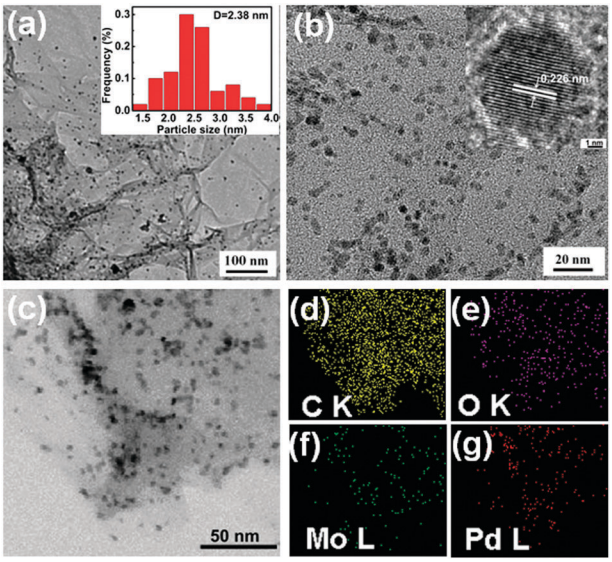

Fig. 1 (a–c) TEM images of Pd/PMo12/rGO at different magnifications. Inset of (a): size distribution of Pd NPs in Pd/PMo12/rGO. Inset of (b): the HRTEM image of Pd NP. Element-mapping images of Pd/PMo12/rGO. (d) C, (e) O, (f) Mo, and (g) Pd.

show that the agglomeration of Pd NPs was efficiently prevented due to the electrostatic repulsive interactions derived by PMo12 anions.[9c,10] In addition, from element-mapping images (Fig. 1d–g), the C, O, Mo, and Pd elements could be obviously observed, which efficiently attest the existence of Pd, PMo12, and rGO in the composite.

The structures of the composite were further characterized by powder X-ray diffraction (XRD), N_2 adsorption–desorption, Fourier transform infrared spectroscopy (FTIR), and Raman spectroscopy. As shown in Fig. S1a (ESI†), a weak and broad peak at about 24° is observed, indicating that GO has been successfully reduced to rGO.[9f,11] The characteristic peaks at 40.2, 46.7, 68.4, 82.4, and 87° are indexed to the (111) (200) (220) (311), and (222) planes of face-centered cubic Pd crystals (JCPDS-87-639). However, there are no noticeable diffraction peaks of PMo12, implying that PMo12 does not exist in the crystalline state, but in the dispersed state with no agglomeration.[9c,12] Fig. S1b (ESI†) reveals that the N_2 adsorption–desorption isotherms and the corresponding pore size distributions of Pd/PMo12/rGO and PMo12/rGO, which are of type IV with distinct hysteresis loops, implying a micro/mesoporous structure. Compared to those of the reported GO,[13] rGO,[14] and POMs,[15] the surface area of porous PMo12/rGO (488 $m^2\ g^{-1}$) increases, suggesting that the successful introduction of POMs breaks the face-to-face stacking of rGO nanosheets.[12,15] Nevertheless, because the pores of PMo12/rGO are occupied by Pd NPs, the surface area of Pd/PMo12/rGO (275 $m^2\ g^{-1}$) is lower than PMo12/rGO.[9b] The pore size distributions of PMo12/rGO and Pd/PMo12/rGO are mainly centered at 3.8 nm on the basis of the Barrett–Joyner–Halenda (BJH) method, which are beneficial to promoting the diffusion of O_2. As seen from FTIR spectra (Fig. S1c and S2, ESI†), the characteristic peaks of PMo12 remain almost unchanged, demonstrating that PMo12 in the Pd/PMo12/rGO composite preserves its Keggin structure. Whereas, the band of P═O of Pd/PMo12/rGO shifts to higher wave numbers attributed to the interactions of Pd NPs and PMo12/rGO.[9f,15] The detailed data are summarized in Table S1 (ESI†). In the Raman spectra (Fig. S1d, ESI†), it is found that the I_D/I_G values of Pd/PMo12/rGO and PMo12/rGO are higher than that of GO, revealing more defects existing in the corresponding samples.[9a]

The electrocatalytic performance of Pd/PMo12/rGO for ORR was examined in a 0.1 M $HClO_4$ solution. As shown in Fig. 2a, the cathodic current density in an O_2-saturated 0.1 M $HClO_4$ solution obviously increases in comparison with that in an N_2-saturated solution, exhibiting an admirable electrocatalytic activity. To further assess the ORR process of the composite, linear sweep voltammograms (LSVs) were performed on a rotating-disk electrode (RDE) at a scan rate of 10 mV s^{-1} and different rotating speeds from 100 to 2500 rpm in an O_2-saturated 0.1 M $HClO_4$ solution. Fig. 2b shows that the current density gradually increases with the increase of the rotating rate because the diffusion rates of electrolytes are accelerated. The onset potential of Pd/PMo12/rGO for the ORR is approximately at 0.6 V *vs.* the Ag/AgCl electrode. Additionally, the corresponding Koutecky–Levich (K–L) plots and the electron transfer numbers for the ORR at different potentials are exhibited in Fig. 2c. The good linearity of K–L plots verifies first-order reaction kinetics for the ORR. According to the K–L equation (Experiment section), the average electron transfer number (n) was calculated to be about 3. Meanwhile, we carried out rotating ring-disk electrode (RRDE) measurement to investigate the ORR catalytic pathways of Pd/PMo12/rGO and Pt–C. It is found that the values of n for Pd/PMo12/rGO and Pt–C catalysts are 3 and 3.98, respectively (Fig. S3 (ESI†)), implying that the Pd/PMo12/rGO involves the "$2e^- + 2e^-$" pathway for the ORR, using H_2O_2 as the intermediate.[16] It is worth noting that, although the onset potential of Pd/PMo12/rGO is similar to those of PMo12/rGO and Pd/rGO, the current density of Pd/PMo12/rGO is higher than PMo12/rGO and Pd/rGO (Fig. 2d) due to the synergistic effect of Pd, PMo12, and rGO, which is slightly lower than commercial Pt–C. Thus, these results efficiently confirm that the Pd/PMo12/rGO catalyst is a promising alternative for ORR in the future.

Published on 30 July 2015. Downloaded by Nanjing Normal University on 09/01/2018 13:04:51.

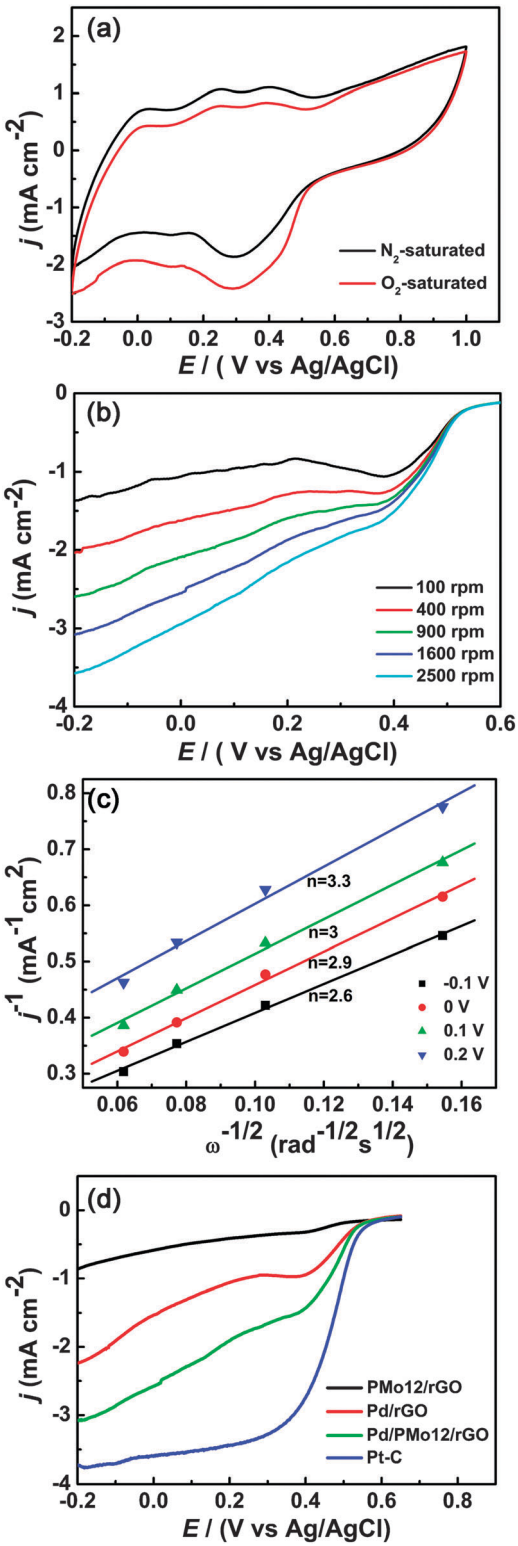

Fig. 2 (a) CVs of Pd/PMo12/rGO in an N_2 or O_2-saturated 0.1 M $HClO_4$ solution; (b) LSVs of Pd/PMo12/rGO at various rotation rates; (c) K–L plots of Pd/PMo12/rGO at various potentials; (d) LSVs of different samples at a rotation rate of 1600 rpm.

In the control experiment, to illustrate the effect of the contents of Pd on the ORR activity, the composites containing different contents of Pd NPs were synthesized, denoted as Pd/PMo12/rGO (*X*) (where *X* stands for the contents of $Pd(NO_3)_2$). From Fig. S4 (ESI†), although the contents of Pd NPs are increased, the onset potential remains unchanged. In contrast, compared to Pd/PMo12/rGO, due to few active species observed from Fig. S5a (ESI†), the Pd/PMo12/rGO (30) catalyst shows slightly lower limiting current density. As for Pd/PMo12/rGO (100), with the increase of the content of $Pd(NO_3)_2$, the Pd NPs were agglomerated into bigger particles (Fig. S5b, ESI†), further decreasing the limiting current density. Thus, it is worthwhile noting that the contents of Pd might be one of the most important issues for the electrocatalytic properties of Pd/PMo12/rGO.

In addition, the methanol-tolerance capacity is an important parameter for the practical applications of DMFCs. As shown in Fig. 3a and Fig. S6, (ESI†), there are noticed ORR signals of Pd/rGO and Pt–C catalysts in LSVs when methanol is added into an O_2-saturated 0.1 M $HClO_4$ solution at a rotation rate of 1600 rpm. On the contrary, for Pd/PMo12/rGO, it is found that the two LSVs almost completely overlap (Fig. 3b), demonstrating that the Pd/PMo12/rGO catalyst has an excellent tolerance to the methanol cross-over effect, superior to that of the commercial Pt–C catalyst, which is very important for practical applications of DMFCs.

Considering the above results, the predominant electrocatalytic activity and methanol-tolerance of Pd/PMo12/rGO may

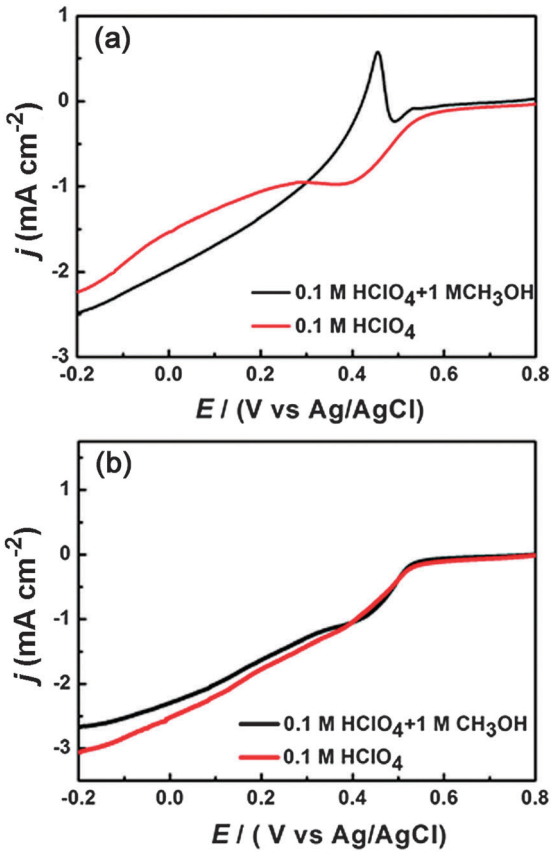

Fig. 3 LSVs of Pd/rGO (a) and Pd/PMo12/rGO (b) in O_2-saturated 0.1 M $HClO_4$ solutions upon addition of methanol at a rotation rate of 1600 rpm.

 This journal is © The Royal Society of Chemistry and the Centre National de la Recherche Scientifique 2016

Published on 30 July 2015. Downloaded by Nanjing Normal University on 09/01/2018 13:04:51.

originate from the following key aspects. (1) rGO, as a support, may boost electronic conductivity and mass transfer.[17] As well, the introduction of well-distributed Pd NPs with small sizes increases the active species, further improving catalytic capacity.[9h] (2) The porous structures and large surface areas, stemming from the interactions of PMo12 and rGO, provide much more sites to uniformly disperse Pd nanoparticles, accessible paths for the approach of O_2 to active sites and simultaneously hinder the contact of methanol and activity sites.[2b] Moreover, PMo12 with high ionic conductivity may be helpful for the capture of oxygen and water molecules, and the dispersibility of rGO.[9b] (3) A synergistic effect of Pd, PMo12, and rGO is beneficial to the above-mentioned performance.

In summary, a novel Pd/PMo12/rGO nanocomposite was prepared by the assistance of PMo12. The structure of the hybrid was characterized in detail, further confirming the successful fabrication of Pd/PMo12/rGO. Pd NPs, as active species, were uniformly distributed over the surfaces of rGO. Porous structures and high ionic conductivity, originating from the interactions of PMo12 and rGO, are beneficial for promoting the diffusion of reactants. Taking advantage of these merits, the composite exhibits better electrocatalytic performance and outstanding methanol-tolerance capacity. The work opens up exciting opportunities for developing multicomponent electrocatalysts as promising candidates for DMFCs.

Experimental

Synthesis of Pd/PMo12/rGO

60 mg of GO was dispersed in 20 mL double-distilled H_2O to form a homogeneous suspension by ultrasonication. And then, 20 mL of $Pd(NO_3)_2$ solution (3 mg L^{-1}) was added into the above solution followed by ultrasonication for 30 min. During the process, the brown-colored product appeared. Subsequently, 20 mL of PMo12 solution (5 mM) and 20 mL of double-distilled H_2O were added into the above solution followed by ultrasonication for 30 min at 30–40 °C. Hydrazine hydrate (1 mL, 80 wt%) was added into the mixture. The solution became black immediately. After 2 h, large particles or solids floating on the liquid surface were obtained, and PMo12 was converted into heteropoly blue (HPB). And then, all solids were centrifuged and washed with water and ethanol to remove byproducts, and dried in a vacuum at 40 °C for 12 h (denoted as Pd/HPB/rGO). The obtained composite was dispersed in 40 mL of double-distilled H_2O and 13 mL of (10 mL H_2O + 3 mL H_2O_2) solution was further added, followed by vigorous stirring for 2 h, and then the solution was kept quiescent for another 12 h. The sample was collected using the above procedures, which are similar to that for HPB/rGO (defined as Pd/PMo12/rGO).

Acknowledgements

This work was financially supported by the NSFC (No. 21371099, 21471080, and 21475062), the program of Jiangsu Specially-Appointed Professor, the NSF of Jiangsu Province of China (No. BK20130043), the Natural Science Research of Jiangsu Higher Education Institutions of China (No. 13KJB150021), the Priority Academic Program Development of Jiangsu Higher Education Institutions, the Natural Science Foundation of Shandong Province (No. ZR2014BQ037), and the Youths Science Foundation of Jining University (No. 2014QNKJ08).

Notes and references

1 (*a*) Y. J. Wang, D. P. Wilkinson and J. Zhang, *Chem. Rev.*, 2011, **111**, 7625; (*b*) X. Zhao, M. Yin, L. Ma, L. Liang, C. Liu, J. Liao, T. Lu and W. Xing, *Energy Environ. Sci.*, 2011, **4**, 2736.
2 (*a*) X. Huang, Z. Zhao, Y. Chen, E. Zhu, M. Li, X. Duan and Y. Huang, *Energy Environ. Sci.*, 2014, **7**, 2957; (*b*) Z. Wen, J. Liu and J. Li, *Adv. Mater.*, 2008, **20**, 743; (*c*) E. Antolini, *ChemPlusChem*, 2014, **79**, 765.
3 (*a*) C. Bianchini and P. K. Shen, *Chem. Rev.*, 2009, **109**, 4183; (*b*) L. Xiao, L. Zhuang, Y. Liu, J. Lu and H. D. Abruña, *J. Am. Chem. Soc.*, 2008, **131**, 602; (*c*) M.-H. Shao, K. Sasaki and R. R. Adzic, *J. Am. Chem. Soc.*, 2006, **128**, 3526.
4 (*a*) D. A. C. Brownson, D. K. Kampouris and C. E. Banks, *Chem. Soc. Rev.*, 2012, **41**, 6944; (*b*) H. Li, S. Pang, S. Wu, X. Feng, K. Müllen and C. Bubeck, *J. Am. Chem. Soc.*, 2011, **133**, 9423; (*c*) D. R. Dreyer, S. Park, C. W. Bielawski and R. S. Ruoff, *Chem. Soc. Rev.*, 2010, **39**, 228.
5 (*a*) P. V. Kamat, *J. Phys. Chem. Lett.*, 2009, **1**, 520; (*b*) C. Huang, C. Li and G. Shi, *Energy Environ. Sci.*, 2012, **5**, 8848.
6 (*a*) L. Cronin and A. Muller, *Chem. Soc. Rev.*, 2012, **41**, 7333; (*b*) D.-Y. Du, J.-S. Qin, S.-L. Li, Z.-M. Su and Y.-Q. Lan, *Chem. Soc. Rev.*, 2014, **43**, 4615; (*c*) D.-L. Long, R. Tsunashima, L. Cronin, D.-L. Long, R. Tsunashima and L. Cronin, *Angew. Chem., Int. Ed.*, 2010, **49**, 1736; (*d*) M. Ammam, *J. Mater. Chem. A*, 2013, **1**, 6291.
7 Z. Kang, Y. Liu, C. H. A. Tsang, D. D. D. Ma, E. Wang and S.-T. Lee, *Chem. Commun.*, 2009, 413.
8 (*a*) S.-X. Guo, Y. Liu, C.-Y. Lee, A. M. Bond, J. Zhang, Y. V. Geletii and C. L. Hill, *Energy Environ. Sci.*, 2013, **6**, 2654; (*b*) M. Jiang, D. Zhu, J. Cai, H. Zhang and X. Zhao, *J. Phys. Chem. C*, 2014, **118**, 14371; (*c*) B. Xia, Y. Yan, X. Wang and X. W. Lou, *Mater. Horiz.*, 2014, **1**, 379.
9 (*a*) R. Liu, S. Li, X. Yu, G. Zhang, S. Zhang, J. Yao, B. Keita, L. Nadjo and L. Zhi, *Small*, 2012, **8**, 1398; (*b*) H. Liu, Y. Zheng, G. Wang and S. Z. Qiao, *Adv. Energy Mater.*, 2015, **5**, 1401186; (*c*) X. Zhao, J. Zhu, L. Liang, C. Liu, J. Liao and W. Xing, *J. Power Sources*, 2012, **210**, 392; (*d*) Y. Ji, L. Shen, A. Wang, M. Wu, Y. Tang, Y. Chen and T. Lu, *J. Power Sources*, 2014, **260**, 82; (*e*) R. Liu, S. Li, X. Yu, G. Zhang, Y. Ma and J. Yao, *J. Mater. Chem.*, 2011, **21**, 14917; (*f*) R. Liu, X. Yu, G. Zhang, S. Zhang, H. Cao, A. Dolbecq, P. Mialane, B. Keita and L. Zhi, *J. Mater. Chem. A*, 2013, **1**, 11961; (*g*) S. Li, X. Yu, G. Zhang, Y. Ma, J. Yao and P. de Oliveira, *Carbon*, 2011, **49**, 1906; (*h*) R. Liu, S. Li, X. Yu, G. Zhang, S. Zhang, J. Yao and L. Zhi, *J. Mater. Chem.*, 2012, **22**, 3319.

10 S. Özkar and R. G. Finke, *J. Am. Chem. Soc.*, 2002, **124**, 5796.
11 G. H. Jeong, S. H. Kim, M. Kim, D. Choi, J. H. Lee, J.-H. Kim and S.-W. Kim, *Chem. Commun.*, 2011, **47**, 12236.
12 S. Wang, H. Li, S. Li, F. Liu, D. Wu, X. Feng and L. Wu, *Chem. – Eur. J.*, 2013, **19**, 10895.
13 D.-D. Zhang, S.-Z. Zu and B.-H. Han, *Carbon*, 2009, **47**, 2993.
14 Y. Si and E. T. Samulski, *Chem. Mater.*, 2008, **20**, 6792.
15 D. Zhou and B.-H. Han, *Adv. Funct. Mater.*, 2010, **20**, 2717.
16 P. S. Ruvinskiy, A. Bonnefont, C. Pham-Huu and E. R. Savinova, *Langmuir*, 2011, **27**, 9018.
17 C. N. R. Rao, H. S. S. R. Matte and K. S. Subrahmanyam, *Acc. Chem. Res.*, 2012, **46**, 149.

Published on 30 July 2015. Downloaded by Nanjing Normal University on 09/01/2018 13:04:51.

 This journal is © The Royal Society of Chemistry and the Centre National de la Recherche Scientifique 2016